Advances in Forest Fire Research

Domingos Xavier Viegas

EDITOR

2014

Degradation modelling of wildland fuels

Mohamad El Houssami[a], Jan Christian Thomas[a], Aymeric Lamorlette[b], Dominique Morvan[b], Albert Simeoni[a]

[a] *BRE Centre for Fire Safety Engineering, Institute for Infrastructure and Environment, School of Engineering, The king's Buildings, The University of Edinburgh, UK m.elhoussami@ed.ac.uk*
[b] *Laboratoire M2P2, UMR 7340 CNRS, Aix-Marseille Universite, Ecole Centrale de Marseille, France*

Abstract

The combustion of forest fuels at laboratory scale is studied by using a Large Eddy Simulation (LES) fire simulator named ForestFireFOAM (FFF), based on the FireFoam package with the addition of a multiphase formulation adapted for highly porous fuel, such as pine needles. Experiments conducted with the FM-Global Fire Propagation Apparatus (FPA) were reproduced with FFF. Arrhenius-type laws were used to model the evaporation and pyrolysis rates. As these laws are temperature-dependent, the mass loss rate and the temperature distribution inside the fuel sample were selected as comparison criteria to better understand the porous fuel heating process using appropriate convective and radiative models and to better describe the burning dynamics of the fuel.

Keywords: Pyrolysis, wildland fuel, FireFOAM

1. Introduction

This study is dedicated to the modelling of the ignition and burning dynamics of pine needle litters. How these moist and highly porous fuels burn represents a fundamental research gap that leads to bigger gaps when it comes to studying their flammability and wildfire spread. This gap hampers the further development of risk indexes and CFD fire spread models. The main goal of this study is to apply a multiphase approach [1–3] that is often used to describe fire propagation [4–6] to the study of piloted ignition of wildland fuels. The multiphase model is based on the resolution of the set of conservation equations governing the time evolution of the coupled system formed by a porous vegetation and its surrounding gas medium, different sub models such as radiation, convection, turbulence, and combustion are included to close the model (Grishin & Albini, 1997). Some of these sub models are not directly relevant for piloted forest fuel ignition modelling at laboratory scale. Such as in (W Mell, Jenkins, Gould, & Cheney, 2007) where a large scale fire spread is started using an ignition line or in (Margerit & Sero-Guillaume, 2002) where an ignition temperature is used. Indeed, the heat and mass transfer processes involved are the same, but the *in situ* conditions lead to a different modelling of these processes due to the underlying assumptions. These assumptions are valid for propagation modelling but not in ignition modelling, since the flow could be laminar during the ignition phase, particularly under no-wind conditions before changing to a turbulent regime. An attempt to correct these models in order to simulate forest fuel ignition has been realised in (Consalvi, Nmira, Fuentes, Mindykowski, & Porterie, 2011). However, ignition procedure was not described thoroughly: The only given assumption was "the criterion for ignition is the thermal runaway in the gas phase: $\frac{\partial^2 T_{g,max}}{\partial t^2} = 0$, where $T_{g,max}$ is the maximum gas temperature at the vicinity of the pilot flame" (Consalvi *et al.*, 2011).

The multiphase formulation was implemented in FireFOAM, a Large Eddy Simulation (LES) solver for fire application, in the C++ object-oriented toolbox of OpenFOAM. The modified solver is called ForestFireFOAM. In addition to presenting the theoretical approach, several strengths and weaknesses

of the current sub-models are identified by comparing simulations to results of fire experiments conducted in the FM-Global Fire Propagation Apparatus (FPA), by burning small samples of dry pine needles exposed to a radiative heat flux. Pine needle beds are used as a reference fuel because they are well characterised in literature and they allow obtaining repeatable fuel bed properties under laboratory settings. Simple modelling of the fuel degradation during the burning of the fuel sample is applied to understand flaming and smouldering. However, in this work the focus is only on heat transfer modelling before and until ignition in order to understand the heating process using appropriate convective and radiative models. It is important to understand this aspect since mass loss rates are highly dependent on the pyrolysis rate, which is usually modelled using an Arrhenius law that is a function of the fuel temperature.

2. Mathematical formulation

2.1. Solid fuel modelling

The solid fuel constituting a forest fuel layer and its interactions with the gas phase are represented by adopting a multiphase formulation [1]. This approach consists in solving the conservation equations (mass, momentum and energy) averaged in a control volume at an adequate scale that contains a gas phase flowing through N solid phases and considering the strong coupling between phases [2]. Here, only one solid phase is considered, and consists of particles of the same geometrical and thermophysical properties, providing the same behaviour. Physico-chemical processes such as pyrolysis, chemical reactions, char oxidation occurring in the solid and gas phases have to be taken into account as well as other phenomena including combustion, radiative and convective heat transfer. The required formulation is made of a set of coupled nonlinear equations, which are presented in (Morvan *et al.*, 2009). The fuel bed is considered as a homogeneous distribution of solid particles whose dimensions and physical properties are evaluated from experimental data. Vegetation state must be characterized using the following set of physical variables: Fuel volume fraction (α_s), fuel density (ρ_s), surface area to volume ratio (σ_s), moisture content (Y_{H2O}), fuel temperature (T_s), and fuel composition.

Adjustments were made in order to better estimate the drag force ($\overline{F_i}$) resulting from the interaction between the gas flow and vegetation, in the momentum equation presented in (Morvan *et al.*, 2009).

$$\overline{F_i} = \rho C_d \frac{\alpha_s \sigma_s}{2} \|\tilde{U}\| \tilde{u}_i \tag{1}$$

The drag force coefficient C_d was averaged and considered constant ($C_d = 0.15$) (Morvan *et al.*, 2009). In this study, it is modelled depending on the mesoscopic Reynolds number, defined as:

$$Re_M = \frac{U}{\nu \sigma_s} \tag{2}$$

where ν represents the air kinematic viscosity. This Reynolds number is compared to a transitional Reynolds number $Re_{M,lim}$ that takes into account the transition from Stokes to inertial flow (Lesieur, 2008). Since an intermediate flow is expected between these two regimes, it is hard to clearly define such a Reynolds number. However, vortices generated by the vortex shedding in the wake of vegetation elements exhibit dislocations responsible for a turbulent break-up (Williamson, 1992). The turbulent flow is then responsible for a constant drag coefficient (Nepf, Sullivan, & Zavitoski, 1997). That is why the Reynolds number accounting for the vortex shedding transition is retained, providing the upper limit for the transition from Darcian to Forchheimer flow. Since the surface area to volume ratio for cylinders of diameter (d) can be define as: $\sigma_s = 4/d$, the transitional Reynolds number for the vortex shedding is evaluated at $Re_{M,lim} \sim 50$ for litters, regarding their typical porosity [10, 11].

For 5% porosity litters:

$$C_d = \begin{cases} \frac{10}{Re_M} \text{ if } Re_M < Re_{M,lim}; \\ C_d = 0.2 \text{ else} \end{cases} \tag{3}$$

For 10% porosity litters:

$$C_d = \begin{cases} \frac{7.5}{Re_M} \text{ if } Re_M < Re_{M,lim}; \\ C_d = 0.15 \text{ else} \end{cases} \tag{4}$$

2.2. Turbulence and combustion

The turbulence model is based on the LES approach developed in the solver OpenFOAM ("OpenFOAM User Guide, OpenFOAM The Open Source CFD Toolbox ," 2010). The turbulent sub-grid scale stress is modelled by the eddy viscosity concept through a one-equation model for the turbulent kinetic energy K (Fureby, Tabor, Weller, & Gosman, 1997), with an additional sink term due to dissipation of sub-grid-scale energy in the canopy (Shaw & Patton, 2003):

$$\frac{D\bar{\rho}K}{Dt} = \frac{\partial}{\partial x_j}\left(\mu_t \frac{\partial K}{\partial x_j}\right) - \bar{\rho}C_d\alpha_s\sigma_s|U|K - C_\varepsilon \frac{\bar{\rho}K^{3/2}}{\Delta} - \rho\overline{u_i''u_j''}\frac{\partial \tilde{u}_i}{\partial x_j} + W \tag{5}$$

$$W = -\frac{\mu_t}{Pr_t\bar{\rho}^2}\frac{\partial \bar{\rho}}{\partial x_j}\frac{\partial \tilde{p}_H}{\partial x_j} \tag{6}$$

$\Delta = (\Delta_x \, \Delta_y \, \Delta_z \,)^{1/3}$ represent the sub-grid filter size, Pr_t represents the turbulent Prandtl number and P_H the hydrodynamic pressure. Most combustion models [5, 12] use Eddy Dissipation Concept (EDC) models for the rate of combustion, which was developed for fully developed turbulent flow.

An extension of the EDC model was proposed (Ren, Wang, & Trouvé, 2013) where the characteristic time scale of fuel-air mixing is different under turbulent and laminar flow conditions. The fuel mass reaction is expressed as:

$$\overline{\dot{\omega}_F'''} = \frac{\overline{\rho}}{\min\left(\frac{k_{sgs}}{C_{EDC}\varepsilon_{sgs}}, \frac{\Delta^2}{C_{diff}\alpha}\right)} \min\left(\tilde{Y}_F, \frac{\tilde{Y}_{O_2}}{s}\right) \qquad (7)$$

where $\tilde{Y}_F$ and $\tilde{Y}_{O_2}$ are the fuel and oxygen mass fraction, α is the thermal diffusicuity, $C_{EDC} = 4$ and $C_{diff} = 10$ [19]. The ratio $\frac{k_{sgs}}{\varepsilon_{sgs}}$ is the turbulent time scale and the ratio $\frac{\Delta^2}{\alpha}$ is the molecular diffusion time scale.

2.3. Convective heat transfer

The term representing the contribution due to convective heat transfer Q_{conv} between hot gases, the flame and the unburned solid fuel is written as follows in the energy balance equation (Morvan *et al.*, 2009):

$$Q_{conv} = \chi(T - T_s) \qquad (8)$$

With T and T_s the gas and solid phase temperatures, respectively. The heat transfer coefficient χ is estimated for low Reynolds numbers, for which independent particle behaviour is observed (Raupach & Thom, 1981), hence the use Hilpert correlation (Incropera, DeWitt, Bergman, & Lavine, 2007) with the Nusselt number:

$$Nu = \frac{\chi D}{K} = C Re^m Pr^{1/3} \qquad (9)$$

Providing the value of χ:

$$\chi = \frac{K}{D} C Re^m Pr^{1/3} \qquad (10)$$

K is the air thermal conductivity and D is the effective diameter equivalent to $4/\sigma_s$. Hence, $Re = 4Re_M$. C and m are coefficients (Incropera *et al.*, 2007) evaluated for a circular cylinder in cross flow. On the basis of the results on momentum absorption found in (Raupach & Thom, 1981), the same relationship and coefficients at low Reynolds are kept, where interactions between solid particles are negligible.

At higher Reynolds, results from (Lamorlette & Collin, 2012) are used to take into account these interactions.

Re < 4   C=0.989   m=0.330

4 < Re < 40   C=0.911   m=0.385

40 < Re < 1560   C=0.683   m=0.466

1560 < Re   C=3.030   m=0.266

2.4. Radiative heat transfer

The term coming from the radiative heat transfer Q_{RAD} can be written as follows:

$$Q_{RAD} = \frac{\alpha_s \sigma_s}{4}[J - 4\sigma T_s^4] \tag{11}$$

$\frac{\alpha_s \sigma_s}{4}$ represents the solid fuel extinction coefficient for spherical particles [17–19]. The total irradiance J is:

$$J = \int_0^{4\pi} I d\Omega \tag{12}$$

Including the contribution of the flames (soot particles) and the embers, the Radiation Transfer Equation (RTE) can be written as follows:

$$\frac{d\alpha_g I}{ds} = \frac{\alpha_s \sigma_s}{4}\left[\frac{\sigma T_s^4}{\pi} - I\right] + \alpha_g \sigma_g \left[\frac{\sigma T^4}{\pi} - I\right] \tag{13}$$

Even if the soot particles in a flame can agglomerate adopting very complex forms, they are assumed spherical ($\Phi = 1\mu m$). The soot field is calculated solving a transport equation for the soot volume fraction, assuming that the production rate of soot particles in the flaming zone is 5% (in mass) of the solid fuel pyrolysis rate. The contribution of soot oxidation is neglected in the flame. Considering that this soot production rate represents the maximum value reached in the under-oxygenated region of the flame, this source term is multiplied by the ratio $(Y_{O2}^* - Y_{O2})/Y_{O2}^*$, representing the deviation from the oxygen concentration at atmospheric conditions. Then, the RTE is solved using a finite volume Discrete Ordinate Method (fvDOM), consisting of the decomposition of the radiation intensity I in a finite number of directions. The irradiance J is calculated by integrating this set of discrete contributions with a numerical Gaussian quadrature (Siegel & Howell, 1992).

3. **Simulations, experiments and discussion**

3.1. **Experimental configuration**

Experiments were performed with the FM Global Fire Propagation Apparatus (FPA), which provides controlled and repeatable conditions. Mass loss rate was measured and the exhaust gases were analysed for composition, heat release rate was deduced by calorimetry [21, 22] and vertical temperature was measured in the sample. Experiments were carried for dry *Pinus resinosa* (Red pine) for two different heat fluxes, 20 and 40 kW/m² with closed baskets and no flow injected in the FPA chamber where the sample holder is located. More details are provided in (Thomas, Everett, Simeoni, Skowronski, & Torero, 2013). The fuel properties are listed in table 1.

Table 1. Fuel properties

Species	$\alpha_s[-]$	$\sigma_s \, [\mathrm{m^{-1}}]$	$\rho_s \, [\mathrm{kg.m^{-3}}]$	$C_p[\mathrm{kJ.kg^{-1}.K^{-1}}]$	$Y_{H2O}[-]$
P. resinosa	0.5	7024	776.6	1800	0.7

3.2. **Numerical conditions**

The set of transport equations in the gas phase are solved using a second order implicit Finite Volume (FV) method. Total Variation Diminishing (TVD) schemes have been adopted to avoid introduction of false numerical diffusion. The set of Ordinary Differential Equations governing the evolution of the solid fuel was solved using a second order explicit method. Two-dimensional calculations are performed to simulate ignition of pine needle litters in the FPA. BlockMesh and snappyHexMesh mesh generators supplied with OpenFOAM, generate robust meshes. However, geometrical complexities and rough edges can easily cause instabilities in the calculations. The pine litter is defined as a rectangular zone with the same dimensions as the sample holder. The pilot flame, located 10 mm above the top of the fuel litter, is represented by an area of size 50 mm x 10 mm providing 2 W to the fluid phase. The flow is simply induced by a pressure differential set at top of the FPA. The mesh is made of 0.8 mm by 0.8 mm square cells in the vicinity of the litter and near the lamps. The mesh is stretched vertically above the lamps and to the top, in order to reduce computational time. The domain geometry is presented in figure 1. Lamps were modelled by walls having the same location and orientation as the real lamps to obtain the same view factor. These walls have very high temperatures (see Table 2 in Results section), adapted in order to obtain the heat flux needed on the sample surface.
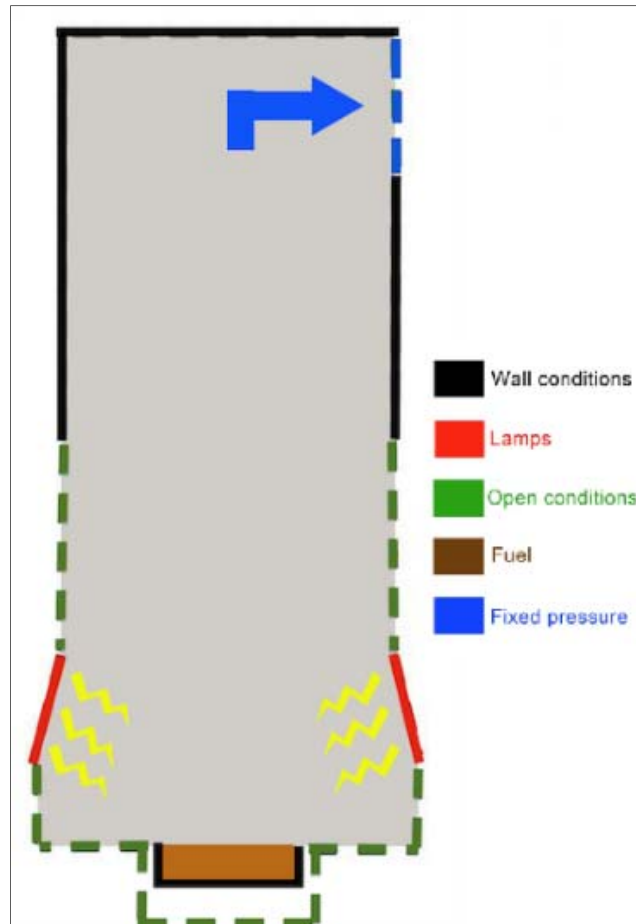
Figure 1. Simulated FPA configuration and boundary conditions

The radiative heat transfer equation is solved for a discrete number of finite solid angles. The accuracy can be increased by using a finer discretisation (Siegel & Howell, 1992):

$$n_{ray} = 4n_{\varphi}n_{\theta} \qquad\qquad (14)$$

where n_{φ} and n_{θ} are the number of discretisation in azimuthal and polar angles, respectively. A sensibility study was carried to determine an adequate amount of discretisation because it is very computationally intensive. $n_{\varphi} = n_{\theta} = 8$ was found to be acceptable, providing a uniformly distributed radiative heat flux at the top of the fuel sample, as observed in the FPA.

3.3. **Results**

The computational time for simulating 10 seconds in parallel on 3 processors was 1h. After conducting a scalability analysis, it was found that the optimal number of cells per processor was 10,000. A snapshot of the temperature field at time $t = 5$ s after ignition is presented in figure 2.
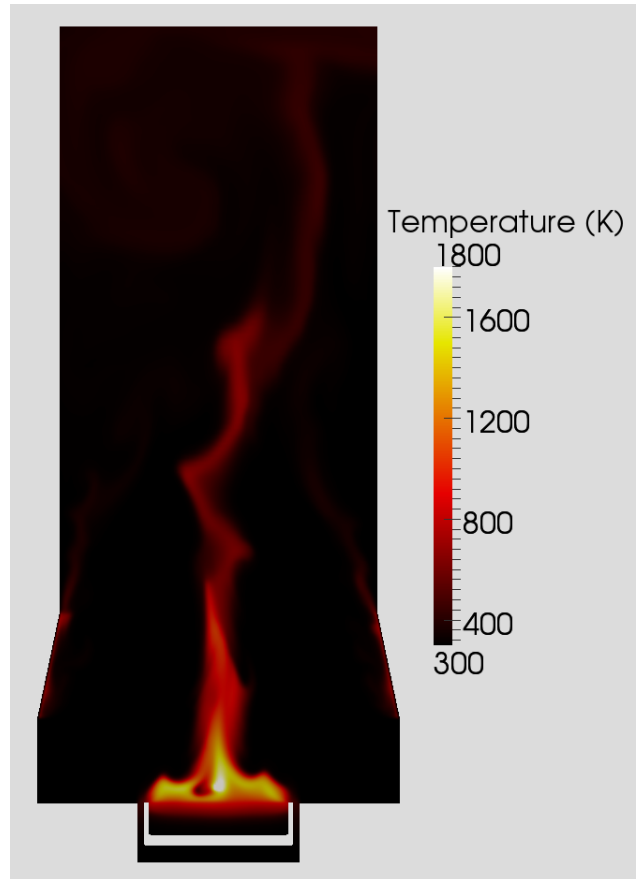
Figure 2. Temperature field 5 seconds after ignition

Preliminary results

In the first attempts to simulate the FPA experiments, the mass loss dropped very quickly. A large number of simulations were conducted to adjust the pyrolysis Arrhenius coefficients in order to have numerical mass loss rates matching the experimental ones. Further simulations were conducted with a maximum pyrolysis rate that could not be exceeded in order to prevent from a rapid mass loss drop. This particular behaviour occurs when the entire fuel is involved in the burning and temperatures become very high, hence the pyrolysis rate increases exponentially. Physically, it represents the fact that pine needles cannot expel all their pyrolysis gases at once. The maximum value of the pyrolysis rate is estimated TGA analysis (Safi, Mishra, & Prasad, 2004) by measuring:

$$\frac{\frac{dm}{dT}}{m} = 0.012 \ K^{-1} \tag{15}$$

with m, the fuel mass and T, the heating temperature. Finally, it was found that the temperature distribution inside the solid fuel was largely over estimated, as presented in figure 3.a and b. Indeed, the simulation for a heat flux of 20 kw/m^2 at the surface of the fuel, temperatures would provide results similar to the experiments done at 40 kw/m^2.
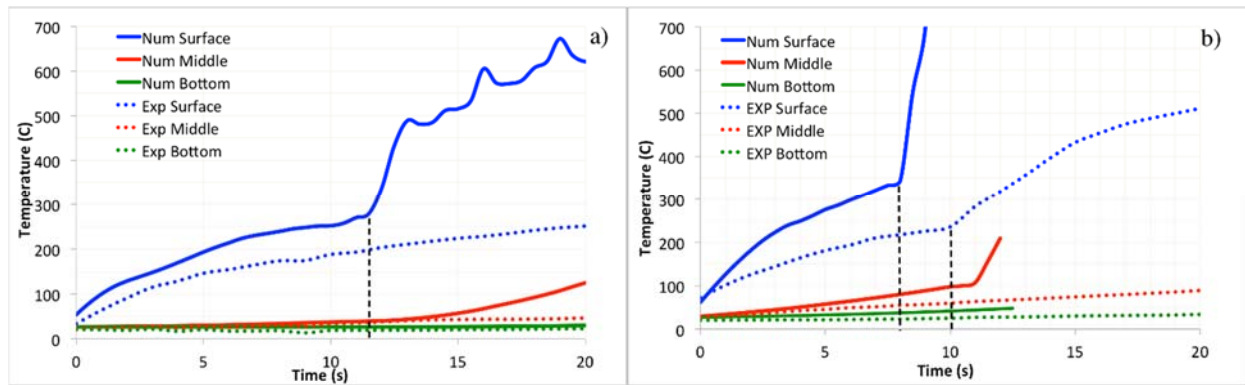
Figure 3. Experimental (dashed) and simulated (solid) temperature distribution in the surface, middle and bottom of the sample with dashed lines representing ignition time a) at 20 kW/m²b) at 40 kW/m².

This was due to the fact that the simulated lamps were assumed to radiate as a black body whereas the FPA heaters operate in very specific spectrum as observed [24, 25] and the fuel emissivity depends on the wavelength number (Monod *et al*., 2009). The halogen lamps of the FPA are very hot and their maximum of emission is shifted towards the lower values of the infrared spectrum, where the absorptivity of the fuels drops dramatically [24]. In consequence, the simulated temperature evolution and ignition times differed from the experiments. Therefore, in order to simulate the experiments performed in the FPA correctly, it was important to estimate the effective absorptivity of the vegetation under the FPA lamps and obtain the correct heat flux absorbed by the fuel.

The absorptivity of vegetation was provided from an experimental study of radiative properties of six vegetal species [18, 26]. Measurements were performed on a large spectrum that covers the spectral radiance spectrum of the FPA infrared heaters, which are very dominant in the near infrared field (0.7-2.5 μm). They can be considered as greybody radiators and the spectral intensity I can be represented by Plank's equation (Marcos Chaos, 2014). The averaged absorptivity is weighted over the normalised spectral radiative intensity at a specific temperature of interest. This temperature is the FPA lamps temperature, corresponding to a specific heat flux (Marcos Chaos, 2014). Simulations were conducted to fit the numerical effective absorptivity to best match the temperature distributions measured in the FPA for 20 kW/m² and 40 kW/m², as shown in figures 4.a and b, respectively. Experimental and numerical effective absorptivities are presented in Table 2. The main difference comes from the fact that the experimental effective absorptivities are obtained for the available species, whereas the numerical are fitted to match FPA experiments on red pine. Another study (Mcallister *et al*., 2012) using halogen/ quartz bulbs shows that the absorptivity of dry lodgepole pine needles is in the same range (0.576) under 50 kW/m² heat flux. The main difference comes from the fact that the experimental effective absorptivities are obtained for the available species, whereas the numerical are fitted to match FPA experiments on red pine.

Table 2. Experimental and numerical effective absorptivities for different heat fluxes

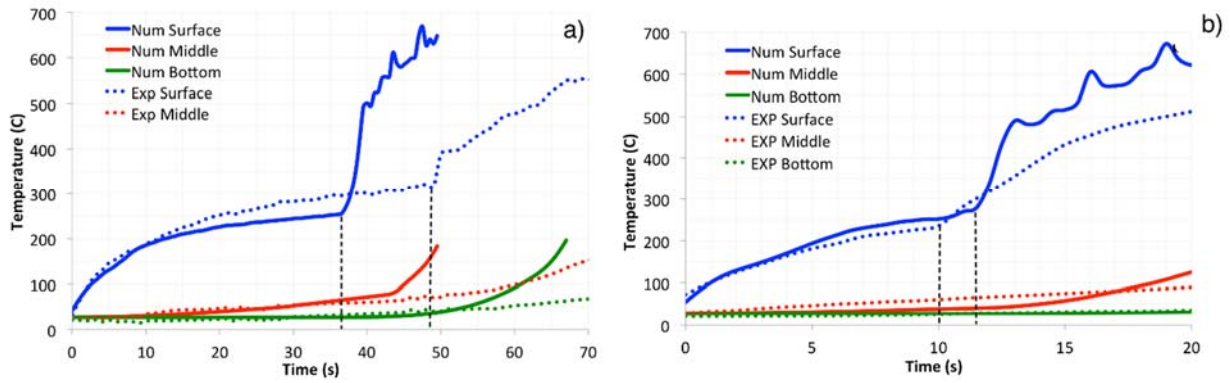| Heat flux (kW/m2)	Lamp Temperatures (K)	Experimental α_{eff}	Numerical α_{eff}
20	820	0.56	0.75
40	900	0.50	0.60

Figure 4. Experimental (dashed) and simulated (solid) temperature distribution in the surface, middle, and bottom of the sample with dashed lines representing ignition time. a) at 20 kW/m²b) at 40 kW/m²

The interesting part of figures 4.a and b covers mainly the temperature variations before ignition, during the heating of the sample only by the lamps of the FPA. In figure 4.a, the temperature evolutions are very similar until the fuel ignites in the simulation 15 seconds before the experiments. The small differences seen in the temperature distribution between experiments and simulations before ignition can be adjusted by modifying the extinction coefficient in equations (11) and (13), as done in (Acem *et al*., 2009). This effect is more pronounced for higher heat fluxes (see figure 4.b). These temperature distributions have large impact on the evaporation and pyrolysis rates, hence on the mass loss rate. The latter are presented for same conditions in figures 5.a and b for 20 kW/m² and for 40 kW/m², respectively.

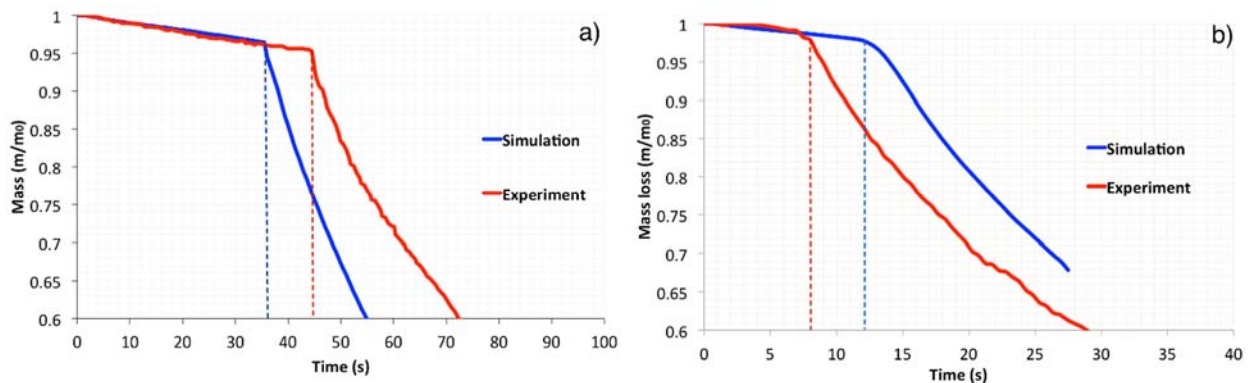*Figure 5. Experimental and simulated mass loss curves for a) 20 kW/m²; b) 40 kW/m². Dashed lines representing ignition time*

The experimental ignition times are not exactly the same in figure 4 as in figure 5, since the experiments had to be done separately. Nevertheless, they have very similar tendencies. Mass loss curves are well reproduced until ignition, regardless of the imposed heat flux, but also right after ignition where pyrolysis is still very dominant. Indeed, if the ignition time is quite different, the slope is the same. It should be noticed that it is very difficult to match ignition times as they are happening due to a conjunction of marginal conditions [28, 29].

4. **Conclusion**

The use of a multiphase model to study the processes involved in piloted ignition of wildland fuels was found to be promising. However, the experimental conditions of the FPA are not easy to simulate. The fuel sample effective absorptivity has to be taken into account in the near infrared field, which is

quite low for pine needles (~ 0.5). The sub-models for the solid phase were able to describe sufficiently the heating (drying and pyrolysis) and ignition processes, including the mass loss rate prior to ignition for two different heat fluxes. Improvements in the models are currently in progress, such as better estimating the radiation extinction coefficient for pine needle litters, analysing pyrolysis gases with a Fourier Transform Infra Red spectroscopy (FTIR) in order to measure pyrolysis production in different conditions. These measured gases will improve the gas phase combustion modelling. Finally, the contribution of the smouldering phase due to char combustion will be studied, which will allow describing the processes involved at the end of the mass loss.

5. Acknowledgment

6. References

A. M. Grishin and F. Albini, A Mathematical Modelling of Forest Fires and New Methods of Fighting Them. Publishing House of the Tomsk University, Tomsk, Russia , 1997.

M. Larini, F. Giroud, B. Porterie, and J. C. Loraud, "A multiphase formulation for fire propagation in heterogeneous combustible media," International Journal of Heat and Mass Transfer, vol. 41, no. 6–7, pp. 881–897, 1998.

D. Morvan, J. L. Dupuy, E. Rigolot, and J. C. Valette, "FIRESTAR: a physically based model to study wildfire behaviour," Forest Ecology and Management, vol. 234S , p. S114, 2006.

O. Séro-Guillaume and J. Margerit, "Modelling forest fires. Part I: a complete set of equations derived by extended irreversible thermodynamics," Int. J.Heat Mass Transfer, vol. 45 , pp. 1705–1722, 2002.

D. Morvan and J. L. Dupuy, "Modelling of fire spread trough a forest fuel bed using a multiphase formulation," Combustion and Flame, vol. 124 , pp. 1981–1994, 2001.

D. Morvan, S. Mèradji, and G. Accary, "Physical modelling of fire spread in Grasslands," Fire Safety Journal, vol. 44, no. 1, pp. 50–61, 2009.

W. Mell, M. A. Jenkins, J. Gould, and P. Cheney, "A physics-based approach to modelling grassland fires," International Journal of Wildland Fire, vol. 16, no. 1, pp. 1–22, 2007.

J. Margerit and O. Sero-Guillaume, "Modelling forest fires. Part II: Reduction to two-dimensional models and simulation of propagation," International Journal of Heat and Mass Transfer, vol. 45, pp. 1723–1737, 2002.

J. L. Consalvi, F. Nmira, A. Fuentes, P. Mindykowski, and B. Porterie, "Numerical study of piloted ignition of forest fuel layer," Proceedings of the Combustion Institute, vol. 33 , pp. 2641–2648, 2011.

M. Lesieur, Turbulence in fluids, Fourth. Springer, 2008.

C. H. K. Williamson, "The natural and forced formation of spot-like 'vortex dislocations' in the transition of a wake," Journal of Fluid Mechanics, vol. 243 , pp. 393–441, 1992.

H. M. Nepf, J. A. Sullivan, and R. A. Zavitoski, "A model for diffusion within an emergent plant canopy," Limnology and Oceanography, vol. 42(8) , pp. 85–95, 1997.

H. Tamura, M. Kiya, and M. Arie, "Vortex shedding from a circular cylinder in moderate-Reynlods-number shear flow," Journal of Fluid Mechanics, vol. 141 , pp. 721–735, 1980.
"OpenFOAM User Guide, OpenFOAM The Open Source CFD Toolbox ." 2010.

C. Fureby, G. Tabor, G. Weller, and D. Gosman, "A comparative study of subgrid scale models in homogeneous isotropic turbulence," Physics of Fluids, vol. 9(5) , pp. 1416–1429, 1997.

R. H. Shaw and E. G. Patton, "Canopy element influences on resolved- and sub-grid-scale energy within a large-eddy simulation," Agricultural and Forest Meteorology, vol. 115 , pp. 5–17, 2003.

W. Mell, A. Maranghides, R. McDermott, and S. L. Manzello, "Numerical simulation and experiments of burning douglas fir trees," Combustion and Flame, vol. 156 , pp. 2023–2041, 2009.

N. Ren, Y. Wang, and A. Trouvé, "Large Eddy Simulation of Vertical Turbulent Wall Fires," Procedia Engineering, vol. 62, pp. 443–452, 2013.

M. R. Raupach and A. S. Thom, "Turbulence in and above plant canopies," Annual Review of Fluid Mechanics, vol. 13 , pp. 97–129, 1981.

F. P. Incropera, D. P. DeWitt, T. L. Bergman, and A. S. Lavine, Fundamentals of Heat and Mass Transfer, vol. 6th. John Wiley & Sons, 2007, p. 997.

A. Lamorlette and A. Collin, "Analytical quantification of convective heat transfer inside vegetal structures," International Journal of Thermal Sciences, vol. 57 , pp. 78–84, 2012.

N. J. De Mestre, E. A. Catchpole, D. H. Anderson, and R. C. Rothermel, "Uniform Propagation of a Planar Fire Front without Wind," Combustion Science and Technology, vol. 65, no. 4–6, pp. 231–244, 1989.

B. Monod, A. Collin, G. Parent, and P. Boulet, "Infrared radiative properties of vegetation involved in forest fires," Fire Safety Journal, vol. 44 , pp. 88–95, 2009.

Z. Acem, A. Lamorlette, A. Collin, and P. Boulet, "Analytical determination and numerical computation of extinction coefficients for vegetation with given leaf distribution," International Journal of Thermal Sciences, vol. 48 , pp. 1501–1509, 2009.

R. Siegel and J. R. Howell, Thermal Radiation Heat Transfer, vol. third ed. . Hemisphere Publishing Corportation , 1992.

C. F. Schemel, A. Simeoni, H. Biteau, J. D. Rivera, and J. L. Torero, "A calorimetric study of wildland fuels," Experimental Thermal and Fluid Science, vol. 32, no. 7, pp. 1381–1389, 2008.

A. Simeoni, J. C. Thomas, P. Bartoli, P. Borowieck, P. Reszka, F. Colella, P. A. Santoni, and J. L. Torero, "Flammability studies for wildland and wildland–urban interface fires applied to pine needles and solid polymers," Fire Safety Journal, vol. 54, no. 0, pp. 203–217, 2012.

J. C. Thomas, J. N. Everett, A. Simeoni, N. Skowronski, and J. L. Torero, "Flammability Study of Pine Needle Beds," in Proc. of the Seventh International Seminar on Fire & Explosion Hazards (ISFEH7), 2013.

M. J. Safi, I. M. Mishra, and B. Prasad, "Global degradation kinetics of pine needles in air," Thermochimica Acta, vol. 412, no. 1–2, pp. 155–162, Mar. 2004.

P. Boulet, G. Parent, Z. Acem, A. Collin, M. Försth, N. Bal, G. Rein, and J. Torero, "Radiation emission from a heating coil or a halogen lamp on a semitransparent sample," International Journal of Thermal Sciences, vol. 77, pp. 223–232, 2014.

Marcos Chaos, "Spectral Aspects of Bench-Scale Flammability Testing: Application to Hardwood Pyrolysis," in Fire Safety Science-Draft Proceedings of the Eleventh International Symposium, 2014.

P. Boulet, "Personal communication 26/02/2014."

S. Mcallister, I. Grenfell, A. Hadlow, W. M. Jolly, M. Finney, and J. Cohen, "Piloted ignition of live forest fuels," Fire Safety Journal, vol. 51, pp. 133–142, 2012.

R. Long, J. Torero, J. Quintiere, and A. Fernandez-Pello, "Scale and transport considerations on piloted ignition of PMMA," in Fire Safety Science - Proceedings of the sixth International Symposium, 1999, pp. 567–578.

J. C. Thomas Simeoni A. Colella F. Torero J.L., "Piloted Ignition Regimes of Wildland Fuel Beds ," 2011.